

disulfide by ketyl, eq 14, the latter formed from excited ketone and mercaptan, eq 13.

Disulfide is reduced to mercaptan when irradiated with benzhydrol in benzene. The quantum yield is low, $\varphi = 0.06$ for 0.012 M disulfide and 0.69 M benzhydrol. A similar quantum yield has been reported for irradiation of diaryl disulfides in a variety of solvents.²⁸ Reduction may result from reaction of excited disulfide with hydrol, or of thiyl radicals from excited disulfide with hydrol, eq 9. If the latter, it is not clear whether the yield of thiyl radicals is low, most of the excited disulfide decaying to ground state, or the yield is high, with most of the thiyl radicals dimerizing. When benzophenone is also present, and is largely quenched by disulfide but in part reacts with benzhydrol to form ketyl radicals, the efficiency of reduction of the disulfide is increased. If direct and sensitized²⁹ excitation of disulfide lead to similar reactivity, it may be estimated that formation of ketyl radical with $\varphi = 0.17$ increased reduction of disulfide with $\varphi = 0.034$, 40% of the ketyl radicals reducing disulfide, eq 14, and/or thiyl radicals which might otherwise have dimerized.

In the benzophenone-benzhydrol system, containing a retarding concentration (~ 0.01 M) of mercaptan disulfide, masking and quenching by the sulfur compounds are sufficient to account for all the observed retardation. Reduction of benzophenone ketyl radical to benzhydrol by mercaptan is not observed in competition with dimerization to benzpinacol. In radiation-induced reactions, products of radiolysis of solvent, reactive radicals, may be largely scavenged by mercaptans, leading to thiyl radicals. The reactive radicals and the thiyl radicals may also react with sensitive solutes, converting them in part to stabilized radicals which may not be repaired by mercaptan. These may enter into coupling reactions and lead to biological damage.

Acknowledgment. This work was supported by the Energy Research and Development Agency (3118).

References and Notes

- (1) Pitts, J. N.; Letsinger, R. L.; Taylor, R. P.; Patterson, J. M.; Recktenwald, G.; Martin, R. B. *J. Am. Chem. Soc.* **1959**, *81*, 1068.
- (2) Bell, J. A.; Linschitz, H. *J. Am. Chem. Soc.* **1963**, *85*, 528.
- (3) Porter, G.; Wilkinson, F. *Trans. Faraday Soc.* **1961**, *57*, 1686.
- (4) Schenck, G. O.; Koltzenberg, G.; Grossman, H. *Angew. Chem.* **1957**, *69*, 177.
- (5) Cohen, S. G.; Cohen, J. I. *Isr. J. Chem.* **1968**, *6*, 757.
- (6) Cohen, W. D. *Recl. Trav. Chim. Pays-Bas* **1920**, *39*, 243.
- (7) Moore, W. M.; Hammond, G. S.; Foss, R. P. *J. Am. Chem. Soc.* **1961**, *83*, 2789.
- (8) Cohen, S. G.; Litt, A. D. *Tetrahedron Lett.* **1970**, 837.
- (9) (a) Cohen, S. G.; Orman, S.; Laufer, D. A. *Proc. Chem. Soc. London* **1961**, 301; (b) *J. Am. Chem. Soc.* **1962**, *84*, 1061, 3905.
- (10) Cohen, S. G.; Laufer, D. A.; Sherman, W. V. *J. Am. Chem. Soc.* **1964**, *86*, 3060.
- (11) Guttenplan, J. B.; Cohen, S. G. (a) *Chem. Commun.* **1969**, 247; (b) *J. Org. Chem.* **1973**, *38*, 2001.
- (12) Zepp, R. G.; Wagner, P. J. *J. Chem. Soc., Chem. Commun.* **1972**, 167.
- (13) Gruen, H.; Schott, H. N.; Byers, G. W.; Giles, H. G.; Kampmeier, J. A. *Tetrahedron Lett.* **1972**, 3925.
- (14) Nakasaki, M. *Nippon Kagaku Zasshi* **1953**, *74*, 405.
- (15) Wang, C. H.; Cohen, S. G. *J. Am. Chem. Soc.* **1959**, *81*, 3005.
- (16) Leo, A.; Westheimer, F. H. *J. Am. Chem. Soc.*, **1952**, *74*, 4383.
- (17) Field, L.; Grunwald, F. A. *J. Org. Chem.* **1951**, *16*, 946.
- (18) Cohen, S. G.; Green, B. *J. Am. Chem. Soc.* **1969**, *91*, 6824.
- (19) Hammond, G. S.; Baker, W. P.; Moore, W. M. *J. Am. Chem. Soc.* **1961**, *83*, 2795.
- (20) Denisov, G. S.; Kazakova, E. M.; Ryl'tsev, E. V. *Chem. Abstr.* **1968**, *69*, 2862.
- (21) Inbar, S.; Cohen, S. G., unpublished results.
- (22) Sherman, W. V.; Cohen, S. G. *J. Phys. Chem.* **1966**, *70*, 178.
- (23) Cohen, S. G.; Rose, A. W.; Stone, P. G. *Isr. J. Chem.* **1977**, *16*, 318.
- (24) Walling, C.; Seymour, D.; Wolfstirn, K. B. *J. Am. Chem. Soc.* **1948**, *70*, 2559.
- (25) Hammond, G. S.; Weiner, S. A. *Intra-Sci. Chem. Rep.* **1969**, *3*, 241.
- (26) Walling, C. *J. Am. Chem. Soc.* **1948**, *70*, 2561.
- (27) Burkhart, R. D. *J. Am. Chem. Soc.* **1957**, *79*, 1924.
- (28) Lyons, W. E. *Nature (London)* **1948**, *162*, 1004.
- (29) Walling, C.; Rabinowitz, R. *J. Am. Chem. Soc.* **1959**, *81*, 1137.

1,2-Di(9-anthryl)ethane. Crystal and Molecular Structure of the Photoisomer. Conformational Effects in the Photophysics and Photochemistry

Bryan F. Anderson,^{1a} James Ferguson,* Masaharu Morita,^{1c} and Glen B. Robertson^{1b}

Contribution from the Research School of Chemistry, The Australian National University, Canberra, A.C.T. 2600, Australia. Received April 26, 1978.

Abstract: Photodissociation of the photoisomer crystal (AEAPI) gives a number of conformations of the 1,2-di(9-anthryl)ethane with different photophysical and photochemical properties. Weakly absorbed light produces two nonfluorescent conformations, with slightly different orientations in the crystal, and two fluorescent conformations which are thermally related. Both sets can be photoisomerized with different rates, at liquid helium temperature. Other, more relaxed, sandwich conformations are produced by more strongly absorbed light and possible conformational arrangements of the two chromophores have been identified by polarized absorption spectra. The crystal and molecular structure of the photoisomer has been determined from single-crystal X-ray diffraction data collected on a Picker FACS-1 diffractometer. Crystals of AEAPI are monoclinic, with $a = 10.095$ (2) Å, $b = 12.471$ (2) Å, $c = 8.340$ (1) Å, $\beta = 111.20$ (1)°, and $Z = 2$. The packing arrangement is strongly pseudocentrosymmetric, approximating space group $P2_1/c$. The structure was solved using the MULTAN programs and has been refined successfully in space group $P2_1$, with one additional (noncrystallographic) constraint, viz., that the two anthracene-derived moieties in each molecule are exactly related by inversion symmetry. Agreement between observed and calculated structure factor amplitudes for the terminal scattering model is only moderate, with weighted and unweighted R factors of 0.36 and 0.08, respectively, for 1776 observed unique data. Nevertheless, bond lengths and bond angles are all close to their expected values, and a number of spectral features can be correlated with the crystal packing arrangement.

Introduction

The reversible photoisomerization of 1,2-di(9-anthryl)ethane (AEA) was studied by Livingston and Wei,² although a description of the two isomers (AEA and its photoisomer

AEAPI) was given first by Roitt and Waters.³ More recently,⁴⁻⁹ there have been studies of the photophysical and photochemical properties of both isomers.

The feature of recent interest is the photodissociation of AEAPI to form AEA, in which the two anthracene chromo-

phores are chemically linked and therefore subject to interactions which depend on their conformational arrangement. If the photodissociation is carried out in a rigid medium, the solvent cage holds the AEA in a face-to-face sandwich conformation, which is not the normal ground-state arrangement. If a rigid glass is used, there is considerable variation in the extent to which relaxation away from the topochemical conformation occurs,⁶ whereas the single crystal of the photoisomer (AEAPI) provides a much more homogeneous environment for the dissociated molecule. In addition, the use of polarized light and a knowledge of the crystal structure of the photoisomer allow deductions to be made about the conformational arrangement of the dissociated molecules. The present paper is concerned with these features.

Experimental Section

The spectroscopic studies were made using a variety of instruments and techniques, described previously.^{6,10} Photodissociation of the photoisomer crystal was effected either by 254-nmHg radiation or by a high-pressure xenon lamp dispersed through a double monochromator (Spex 1402 or Zeiss 12 MM). The wavelength of the photocleavage light determines the concentration gradient of the cleaved molecules in the crystal and is therefore an essential experimental variable.¹¹ The rate of the thermal dissociation of the AEAPI molecule was measured with a Cary 17 spectrophotometer. The solvent was *n*-hexane contained in a square cross section silica cell and air was removed from the solution by freeze-thaw cycles before sealing the tube. Silicone oil was used as a high-temperature thermostating fluid to measure the temperature dependence of the rate.

The photoisomer crystals were grown from either dichloromethane or benzene-methylcyclohexane. In the former the well-developed face is predominantly (010), while it is completely (100) in the latter. The crystals are unstable and it is therefore necessary to use freshly prepared crystals, especially for measurements of fluorescence spectra. When we allowed the AEAPI to stand for a few days, even in a refrigerator, there was thermal decomposition of the AEAPI and a relaxed form of AEA was produced in the lattice.

Crystals of the photoisomer grow as clear colorless rods elongated along *a*, which turn milky yellow on exposure to X-rays. Preliminary precession photographs showed the crystal to be monoclinic. No systematic absences were observed although reflections of index type $0k0$, $k = 2n + 1$, and $h0l$, $l = 2n + 1$, were uniformly weak. Precise cell dimensions were determined by least-squares minimization from the diffractometer-centered setting angles of 12 widely separated reflections with $33^\circ < 2\theta < 49^\circ$.¹²

Crystal Data. C₃₀H₂₂; fw 382 daltons; monoclinic; $a = 10.095$ (2) Å, $b = 12.471$ (2) Å, $c = 8.340$ (1) Å; $\beta = 111.20$ (1)°; space group $P2_1$; D_m (by flotation in aqueous KI) = 1.30 g cm⁻³; $Z = 2$; $D_c = 1.296$ g cm⁻³; $\lambda(\text{Mo K}\alpha) = 0.70926$ Å; $F(000) = 404$ e⁻.

Reflection data were collected on a Picker FACS-1 automated four-circle diffractometer in the θ - 2θ mode with graphite monochromated (monochromator $2\theta = 12.16^\circ$) molybdenum $K\alpha$ radiation. Each reflection was scanned (at a rate of $2^\circ/\text{min}$) from 1° below the calculated position of the $K\alpha_1$ maximum to 1° beyond that of the $K\alpha_2$ peak, and stationary background measurements were counted for 10 s at either end of the scan range. Three reflections (0 12 0, $\bar{3}$ 0 8, $\bar{8}$ 1 1) were monitored every 50 data as a check on instrument instability and, more importantly, crystal decomposition. Under irradiation the photoisomer crystals decompose quite rapidly and an average decrease of over 20% in the standard intensities had invariably occurred within 18 h of the start of data collection. A series of five crystals (all with approximate dimensions $0.05 \times 0.02 \times 0.03$ cm, and having similar prior exposure to radiation), each mounted with the ϕ goniometer axis parallel to the longer *a* axial direction, was used to collect the unique set of data $-h k \pm l$, $3^\circ \leq 2\theta \leq 55^\circ$. Crystals were renewed after the average decrease in the intensity of the standard reflections had reached about 25%.

Individual data sets were corrected separately for crystal degradation and were subsequently placed on a common scale by comparison of the mean corrected intensities of the standard reflections. Reflection intensities were then corrected for Lorentz and polarization effects and the corrected structure amplitudes $|F_o|$ ¹³ were assigned individual estimated standard deviations $\sigma(F_o)$,¹⁴ with instrumental uncertainty constant $\rho^{2,15}$ equal to 0.002. Reflections with uneven backgrounds [$|B_1 - B_2| \geq 3(B_1 + B_2)^{1/2}$] were discarded, as were

those considered unacceptably weak [$I \leq 3\sigma(I)$]. After sorting and averaging equivalent reflections, 1776 unique data were obtained. Of these, 50 reflections ($|F|_{\text{max}} = 8.5$ e⁻) contravened the glide extinction and 6 reflections ($|F|_{\text{max}} = 3.5$ e⁻) contravened the screw axis extinction in space group $P2_1/c$. Reflection intensities were not corrected for specimen absorption effects.

Because intensity statistics for the data set strongly indicated the space group was centrosymmetric, initial attempts to solve the structure involved applying the direct phasing program MULTAN¹⁶ to the space groups $P2/m$, $P\bar{1}$, and then $P2_1$, Pm , and $P1$. It was only when the anomalous reflections were ignored, and phasing was carried out for space group $P2_1/c$, that a meaningful *E* map was obtained. All 16 atoms in half a molecule of [2,2](9,10)anthracenophane photoisomer could be identified in the Fourier synthesis, although comparison of the measured crystal parameters with those published¹⁷ for the symmetric photoisomer assured us that our compound was not the same. Full-matrix least-squares refinement in space group $P2_1/c$ with all atoms anisotropic and the bridging group atoms [C(15) and C(16); see Figure 1] assuming half-occupancies reduced the conventional *R* value to 13%. Atom scattering factors from International Tables¹⁸ were used throughout for solution and refinement of the structure. Bond lengths and angles and all temperature factors appeared to be quite normal. The nine largest peaks ($0.4e^- - 0.7e^-$) in the difference map occurred at locations expected for the aromatic hydrogens and some of the smaller maxima could also be correlated with the methylene protons. After inclusion of hydrogen atoms (isotropic thermal parameters, methylene hydrogens by calculation), the refinement converged with $R_1 = \sum ||F_o| - |F_c|| / \sum |F_o| = 0.093$ and $R_2 = (\sum \omega ||F_o| - |F_c||^2 / \sum \omega |F_o|^2)^{1/2} = 0.21$ with $\omega = \sigma(F_o)^{-2}$.

Refinement was continued in space group $P1$ with the positional and thermal parameters of the atoms in the four half-molecules coupled to maintain strict $P2_1/c$ symmetry, while the occupancy factors for the four C(15), C(16) pairs at (x, y, z) , $(-x, -y, -z)$, $(x, 1/2 - y, 1/2 + z)$, and $(-x, 1/2 + y, 1/2 - z)$ were allowed to vary. The atoms (x, y, z) and $(\bar{x}, \bar{y}, \bar{z})$ and the atoms $(x, 1/2 - y, 1/2 + z)$ and $(-x, 1/2 + y, 1/2 - z)$ were coupled so that (a) bonded pairs were constrained to equal occupancy and (b) sums of occupancies of symmetry-related pairs [(x, y, z) , $(\bar{x}, \bar{y}, \bar{z})$, etc.] were constrained to unity. The occupancy factor for the (x, y, z) set oscillated about 1, so the atoms C(15) and C(16) at position $(\bar{x}, \bar{y}, \bar{z})$ were removed and those at (x, y, z) were given full occupancy. Occupancy factors for the C(15), C(16) sets at $(x, 1/2 - y, 1/2 + z)$ and $(-x, 1/2 + y, 1/2 - z)$ remained close to 0.5. At convergence all shifts, except for occupancy factors for the coupled $(x, 1/2 - y, 1/2 + z)$ and $(-x, 1/2 + y, 1/2 - z)$ methylene groups, were less than 0.5 times their estimated standard deviation. For the coupled methylene groups, the final occupancy factors were 0.52 and $1 - 0.52$ and the shift to esd ratio was 0.76. Final values for R_1 and R_2 were 0.082 and 0.20, respectively.

However, the model described above implies that, within the crystal, one set of molecules (those about position (0, 0, 0) in the chosen crystal unit cell) always packs in a preferred orientation, while the second set, about $(0, 1/2, 1/2)$, orients randomly. Such a situation seems physically unreal and it is hard to understand how the different lattice sites could be differentiated during the crystallization process. It seemed more probable that the model had refined to a false minimum and that the packing arrangement actually conforms closely to that expected for an ordered arrangement of molecules in space group $P2_1$.

Accordingly, the occupancy factors for the above model were changed and refinement in $P2_1$ was commenced. Parameters for the bianthracene moieties were, however, still coupled to maintain the essential $P2_1/c$ symmetry and only the methylene bridges and the associated protons had the 2_1 relationship. At convergence all parameter shifts were less than half their estimated standard deviations with $R_1 = 0.085$ and $R_2 = 0.36$. A final difference synthesis shows no maxima greater than $0.4e^-$ and none of these occur at locations which would suggest the presence of possibly disordered atoms. For completeness the model was also refined in space group Pc ; corresponding *R* values were 0.088 and 0.20.

Unfortunately, the results described above do not provide an unambiguous answer except that exact inversion disordering, as would be implied by the $P2_1/c$ space group, is ruled out absolutely by the large number of observed reflections which violate the glide extinction. Our preference for $P2_1$ rather than Pc derives from the same considerations. It does not, of course, account for the violations of the screw axis extinction and, in addition, differences between observed and calculated structure factors in the $P2_1$ refinement are still, in many instances, quite large. While some of this may be attributed to the

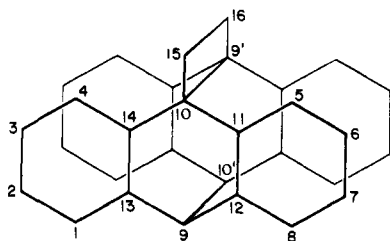


Figure 1. 1,2-Di(9-anthryl)ethane photoisomer (AEAPI): atom nomenclature.

susceptibility of the crystals to X radiation and the consequent need to use five crystals during data collection, it is disappointing to find that those $h0l$ reflections with $l = 2n + 1$ show rather worse agreement than the bulk of the data. The presence of the pseudocenters of symmetry at $(0, 0, 0)$ and $(0, \frac{1}{2}, \frac{1}{2})$ so dominates the structure that sensible refinement is only possible with the two anthracene-derived moieties in each molecule constrained to be related exactly by inversion symmetry. The symmetry operations of space group $P2_1$ require no such constraint and it may be just such deficiencies in the scattering model which are responsible for the poor agreement. It is to be noted, however, that the extent to which the actual structure differs from this model must be quite small since there are no obvious anomalies in the refined anisotropic temperature parameters.

Description of the Structure. The chemical formula and the numbering system used with the 1,2-di(9-anthryl)ethane photoisomer are shown in Figure 1 and a stereoscopic view of the molecule drawn from the X-ray determined coordinates (Table I) is presented in Figure 2. Atomic thermal parameters (Table III) and a listing of the observed and calculated structure amplitudes (Table IV) have been deposited and appear in the microfilm edition (see paragraph at end of paper). Although the crystal structure was refined finally in space group $P2_1$, the two molecules in the unit cell are placed about the lattice points, $(0, 0, 0)$ and $(0, \frac{1}{2}, \frac{1}{2})$, which act as exact centers of symmetry for the bianthracene moieties. The atoms with dashed numbers are thus assumed to be centrosymmetrically related to their undashed counterparts as in space group $P2_1/c$.

Bond lengths and interbond angles are presented in Table II. Although the final R values are not particularly good and some features of the refinement were unsatisfactory, the estimated standard deviations on carbon-carbon bond lengths within the centrosymmetric part of the molecule are all about 0.0035 \AA and in most instances equivalent bonds are within three times this value of the mean. Standard deviations for the ethylene bridge carbons are 0.005 and 0.007 \AA . The error on interbond angles is about 0.2° . The bonds formed by photoisomerization ($C(9)-C(10')$ $1.642(3) \text{ \AA}$) are longer than the usual $C_{sp^3}-C_{sp^3}$ distance but well within the limits reported for similar photoisomerized structures ($1.61-1.77 \text{ \AA}$).^{17,19-21} Within the cyclobutane ring, the bonds $C(9')-C(16)$ and $C(10)-C(15)$ (mean $1.442(3) \text{ \AA}$) are considerably shorter than the expected $1.537(5) \text{ \AA}$,^{22a} although the $C(15)-C(16)$ bond ($1.527(7) \text{ \AA}$) is normal. The in-ring angles within the cyclobutane are all close to 90° with those at $C(9)$ and $C(10)$ being slightly less than the right angle.

Bonds within the two independent aromatic rings vary between $1.364(4)$ and $1.405(3) \text{ \AA}$ with a mean of 1.384 \AA , while the endocyclic angles average to 120.0° . Carbon-hydrogen bonds are satisfactory as are the C-H exocyclic angles (mean values 0.99 \AA and 120°). Both aromatic rings are strictly planar within the limits of the data, with ring $C(13)-C(1)-C(4)-C(14)$ having the plane equation $-0.1642X + 0.6868Y - 0.7080Z + 0.8019 = 0$,²³ and ring $C(11)-C(5)-C(8)-C(12)$ having the plane equation $0.6070X + 0.5716Y - 0.5521Z + 0.7638 = 0$. The associated hydrogens in the main do not deviate significantly from these calculated mean planes ($\Delta \leq 3\sigma$). Atoms $C(9)$ and $C(10)$, however, are not co-planar with either of the phenyl rings but lie slightly below both planes toward the center of the molecule [$C(9)$ maximum deviation 0.053 \AA ; $C(10)$ maximum deviation 0.046 \AA], a consequence no doubt of the strained $C(9)-C(10')$ photoisomerization bonds. The angle between the normals to the two aromatic rings (46.9°) is very similar to that found by Ehrenberg¹⁷ for the $[2.2](9,10)$ anthracenophane photoisomer (47.33°) and only slightly less than that found by Ferguson et al.¹⁹ for the anthracene-tetracene photoisomer (48.04°). The central nonaromatic ring has $C_{sp^2}-C_{sp^3}$ bonds in good agreement with the

Table I. Fractional Atomic Positional Parameters for AEAPI^a

atom	X/A	Y/B	Z/C
CA(1)	-0.2012 (2)	0.0040 (2)	0.2344 (3)
CA(2)	-0.3303 (2)	-0.0478 (2)	0.1872 (3)
CA(3)	-0.3630 (3)	-0.1270 (2)	0.0627 (3)
CA(4)	-0.2676 (2)	-0.1533 (2)	-0.0135 (3)
CA(5)	0.2159 (3)	-0.2075 (2)	0.0996 (4)
CA(6)	0.3457 (3)	-0.2073 (3)	0.2291 (5)
CA(7)	0.3789 (3)	-0.1294 (3)	0.3533 (4)
CA(8)	0.2807 (3)	-0.0496 (2)	0.3477 (4)
CA(9)	0.0363 (2)	0.0350 (2)	0.1974 (3)
CA(10)	-0.0285 (2)	-0.1239 (2)	-0.0491 (3)
CA(11)	0.1162 (2)	-0.1286 (2)	0.0911 (3)
CA(12)	0.1487 (2)	-0.0488 (2)	0.2170 (3)
CA(13)	-0.1043 (2)	-0.0210 (2)	0.1578 (2)
CA(14)	-0.1371 (2)	-0.1017 (2)	0.0320 (2)
CA(15)	-0.0567 (6)	-0.2063 (4)	-0.1793 (6)
CA(16)	-0.0769 (7)	-0.1225 (4)	-0.3186 (5)
HA(1)	-0.174 (2)	0.055 (2)	0.315 (3)
HA(2)	-0.401 (3)	-0.030 (2)	0.238 (4)
HA(3)	-0.455 (2)	-0.157 (2)	0.037 (3)
HA(4)	-0.296 (3)	-0.207 (2)	-0.111 (4)
HA(5)	0.188 (4)	-0.258 (3)	0.004 (5)
HA(6)	0.431 (3)	-0.260 (2)	0.242 (3)
HA(7)	0.477 (4)	-0.123 (2)	0.442 (4)
HA(8)	0.297 (3)	0.004 (2)	0.431 (3)
HA(9)	0.029 (4)	-0.247 (3)	-0.153 (5)
HA(10)	-0.153 (4)	-0.247 (3)	-0.193 (5)
HA(11)	-0.180 (4)	-0.120 (3)	-0.377 (4)
HA(12)	0.000 (5)	-0.142 (4)	-0.352 (6)
HA(13)	0.065 (5)	0.084 (5)	0.310 (6)
HB(13)	0.050 (5)	0.192 (4)	0.120 (5)

^a The anisotropic thermal parameters are of the form $\exp[-(\beta_{11}h^2 + \beta_{22}k^2 + \beta_{33}l^2 + 2\beta_{12}hk + 2\beta_{13}hl + 2\beta_{23}kl)]$.

values expected for this type of bond ($1.505(5) \text{ \AA}$).^{22b} The angles at the sp^2 -hybridized carbons have all been reduced from the trigonal value by about 3° at the expense of the adjacent exocyclic angle, while those at the tetrahedral carbons remain close to the expected value. At both $C(9)$ and $C(10')$ it is the exocyclic angles which have deformed to accommodate the distortion to 90° that is found in the cyclobutane.

Photodissociation of AEAPI by Weakly Absorbed Light

The wavelength of the photodissociating light is a factor which directly controls the local environment of the dissociated molecule, through the extent to which the host lattice is disrupted by the production of the dissociated molecules.¹¹ Nearly uniform concentrations of approximately 1 dissociated molecule per 1000 host molecules can be obtained by using a narrow band of wavelengths on the extreme long-wavelength edge of the absorption band of the crystal. The absorption spectrum obtained under these conditions has an intensity distribution which is reproducible from sample to sample, provided the crystals are freshly prepared. These are the bands labeled A_n and B_n in Figure 1 of the earlier report.⁶ The intensity of band C is very dependent on the wavelength of the photodissociating light, being essentially zero for the conditions just given. These conditions provide the maximum constraint by the host lattice.

Earlier,⁶ the absorption spectrum of the photodissociated molecules was assigned to overlapping contributions from two different conformations, A and B. However, after measurements were made of the corresponding excitation spectra it was found that the absorption and excitation spectra did not coincide, so that an analysis of the absorption spectrum was not so straightforward. The presence of the nonfluorescent molecules implies that these molecules are photoisomerizable and subsequent irradiation should remove them from the crystal preferentially. However, experiments soon established

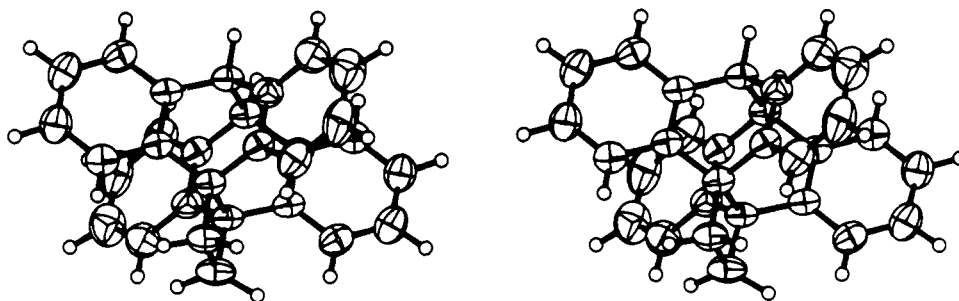


Figure 2. Stereoscopic view of AEAPI.

Table II. Bond Lengths and Interbond Angles for 1,2-Di(9-anthryl)ethane Photoisomer

(a) Bond Lengths, Å							
C(1)–C(2)	1.379 (4)	C(5)–C(6)	1.364 (4)	C(9)–C(12)	1.508 (3)	C(11)–C(12)	1.397 (3)
C(1)–C(13)	1.384 (4)	C(5)–C(11)	1.391 (4)	C(9)–C(13)	1.507 (3)	C(13)–C(14)	1.405 (3)
C(1)–H(1)	0.89 (2)	C(5)–H(5)	0.98 (4)	C(9)–C(10')	1.642 (3)	C(15)–C(16)	1.527 (7)
C(2)–C(3)	1.384 (4)	C(6)–C(7)	1.370 (5)	C(9')–C(16)	1.443 (5)	C(15)–H(9)	0.96 (5)
C(2)–H(2)	0.99 (3)	C(6)–H(6)	1.06 (3)	C(9)–H(13)	1.07 (5)	C(15)–H(10)	1.06 (4)
C(3)–C(4)	1.371 (4)	C(7)–C(8)	1.394 (5)	C(10)–C(11)	1.506 (3)	C(16)–H(11)	0.98 (4)
C(3)–H(3)	0.95 (2)	C(7)–H(7)	1.00 (3)	C(10)–C(14)	1.507 (4)	C(16)–H(12)	0.95 (6)
C(4)–C(14)	1.391 (3)	C(8)–C(12)	1.383 (3)	C(10)–C(15)	1.441 (5)		
C(4)–H(4)	1.01 (3)	C(8)–H(8)	0.93 (3)	C(10')–H(14)	1.02 (5)		
(b) Interbond Angles, Deg							
C(2)–C(1)–C(13)	121.1 (2)	C(12)–C(8)–H(8)	116 (2)	C(8)–C(12)–C(9)	124.3 (2)	C(8)–C(12)–C(11)	119.0 (2)
C(2)–C(1)–H(1)	123 (2)	C(10')–C(9)–C(12)	112.2 (2)	C(8)–C(12)–C(11)	119.0 (2)	C(9)–C(12)–C(11)	116.7 (2)
C(13)–C(1)–H(1)	115 (2)	C(10')–C(9)–C(13)	111.3 (1)	C(9)–C(12)–C(11)	116.7 (2)	C(1)–C(13)–C(9)	124.1 (2)
C(1)–C(2)–C(3)	119.5 (3)	C(10)–C(9')–C(16)	86.6 (2)	C(1)–C(13)–C(9)	124.1 (2)	C(1)–C(13)–C(14)	119.4 (2)
C(1)–C(2)–H(2)	122 (2)	C(10')–C(9)–H(13)	102 (3)	C(9)–C(13)–C(14)	116.4 (2)	C(4)–C(14)–C(10)	124.3 (2)
C(3)–C(1)–H(2)	118 (2)	C(12)–C(9)–C(13)	108.3 (2)	C(4)–C(14)–C(10)	124.3 (2)	C(4)–C(14)–C(13)	118.7 (2)
C(2)–C(3)–C(4)	120.1 (2)	C(12')–C(9')–C(16)	115.8 (3)	C(10)–C(15)–C(16)	91.2 (4)	C(10)–C(15)–H(9)	107 (2)
C(2)–C(3)–H(3)	113 (2)	C(12)–C(9)–H(13)	110 (3)	C(10)–C(15)–H(9)	107 (2)	C(10)–C(15)–H(10)	111 (2)
C(2)–C(3)–H(3)	126 (2)	C(13')–C(9')–C(16)	120.7 (3)	C(16)–C(15)–H(9)	113 (3)	C(16)–C(15)–H(10)	112 (2)
C(3)–C(4)–C(14)	121.1 (2)	C(13)–C(9)–H(13)	113 (3)	C(15)–C(16)–H(11)	103 (2)	H(9)–C(15)–H(10)	120 (3)
C(3)–C(4)–H(4)	119 (2)	C(9')–C(10)–C(11)	112.3 (2)	C(9')–C(16)–C(15)	93.2 (3)	C(9')–C(16)–H(11)	108 (2)
C(14)–C(4)–H(4)	119 (2)	C(9')–C(10)–C(14)	111.7 (2)	C(9')–C(16)–H(11)	108 (2)	C(9')–C(16)–H(12)	110 (3)
C(6)–C(5)–C(11)	120.6 (3)	C(9')–C(10)–C(15)	88.6 (2)	C(15)–C(16)–H(12)	99 (3)	H(11)–C(16)–H(12)	135 (4)
C(6)–C(5)–H(5)	124 (2)	C(9)–C(10')–H(14)	101 (3)				
C(11)–C(5)–H(5)	116 (2)	C(11)–C(10)–C(14)	108.5 (2)				
C(5)–C(6)–C(7)	120.2 (3)	C(11)–C(10)–C(15)	115.3 (3)				
C(5)–C(6)–H(6)	126 (1)	C(11')–C(10')–H(14)	111 (2)				
C(7)–C(6)–H(6)	113 (1)	C(14)–C(10)–C(15)	119.2 (3)				
C(6)–C(7)–C(8)	120.3 (2)	C(14')–C(10')–H(14)	112 (3)				
C(6)–C(7)–H(7)	121 (2)	C(5)–C(11)–C(10)	123.4 (2)				
C(8)–C(7)–H(7)	118 (2)	C(5)–C(11)–C(12)	119.8 (2)				
C(7)–C(8)–C(12)	120.2 (3)	C(10)–C(11)–C(12)	117.0 (2)				
C(7)–C(8)–H(8)	123 (1)						

that the fluorescent molecules were also photoisomerizable, but at a slower rate, so that irradiation eventually removed all of the previously photodissociated molecules. This latter rate was about 0.08 of the former rate, so that careful monitoring of the irradiation time allowed the preferential removal of the nonfluorescent molecules almost completely.

The experimental arrangement¹⁰ allowed a series of experiments to be carried out without the need to change the position of the sample, or its temperature, so that the absorption spectrum of a crystal could be measured before and after a series of photochemical exposures to light. In this way difference spectra provided exactly, without base-line errors, the absorption spectra of the photoactive molecules involved in each irradiation. Initially, irradiation on the extreme absorption edge of the AEAPI crystal gave, typically, the spectra shown in Figures 3a and 4a, for light incident on the (100) and (010) faces, respectively.

Corresponding excitation spectra indicated that the non-fluorescent molecules absorb most strongly at 378 nm (26 450

cm⁻¹) and irradiation at this wavelength for a short time removed these molecules preferentially. The difference spectra then provided the absorption spectra of the nonfluorescent molecules and these are shown in Figures 3b and 4b. Longer irradiation removed these molecules almost completely, leaving the fluorescent molecules; their spectra are given in Figures 3c and 4c.

The photodissociated AEAPI molecule will relax, so far as is possible, to relieve the repulsive forces imposed by the close face to face contact of the anthracene moieties and the strain in the ethane bridge. The necessary motions are (1) a return to planarity of each anthracene moiety and (2) an opening of the face to face contact of these moieties, about the ethane bridge. In addition, the dissociated molecule will probably adjust its position in the crystal to minimize the repulsive interactions between it and its neighbor photoisomer molecules. Here, the distribution of the ethane bridges on neighboring molecules should determine the molecular movements, if any.

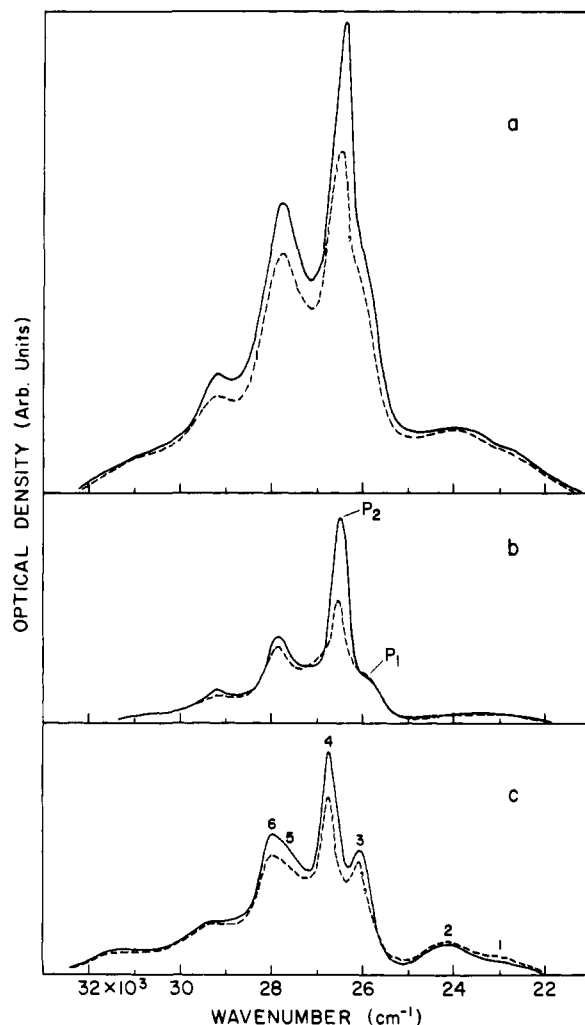


Figure 3. Absorption spectra (10K) of AEA in AEAPI for light incident normal to the (100) face: (a) absorption spectra after initial photodissociation; (b) absorption spectra of nonfluorescent AEA; (c) absorption spectra of fluorescent AEA. Full lines, polarization $\parallel c$; broken lines polarization $\parallel b$.

An analysis of the spectra in Figures 3 and 4, using these ideas, requires knowledge of the projections of the molecules onto the (100) and (010) faces, respectively, and they are shown in Figures 5 and 6.

We consider the nonfluorescent molecules first, the spectra of which are shown in Figures 3b and 4b. There appear to be two sets of molecules, whose main bands are labeled P_1 and P_2 , with the latter dominant. From Figure 3b we observe that the set P_1 is essentially unpolarized in the (100) face, while the set P_2 appears more strongly $\parallel c$ than $\parallel b$ by nearly 2:1. From Figures 4b and 6 we also observe that both P_1 and P_2 are polarized along the short in-plane axis of the photodissociated anthracene moieties, consistent with the 1L_a character of the excited states of these chromophores. This polarization direction means that, returning to Figures 3b and 5, we can assign P_1 to dissociated molecules which retain the orientation of the photoisomer, i.e., a symmetric dissociation with no adjustment of molecular orientation in the lattice. These molecules would be expected to have absorption spectra which are unpolarized in the (100) face for a short axis 1L_a transition in the anthracene chromophore. On the other hand, the set of molecules P_2 has a polarization, in this face, which is consistent with a rotation of the dissociated molecule by 7 or 8° toward the c axis, about an axis normal to the (100) face. We can see immediately from Figure 5 that this is the direction toward

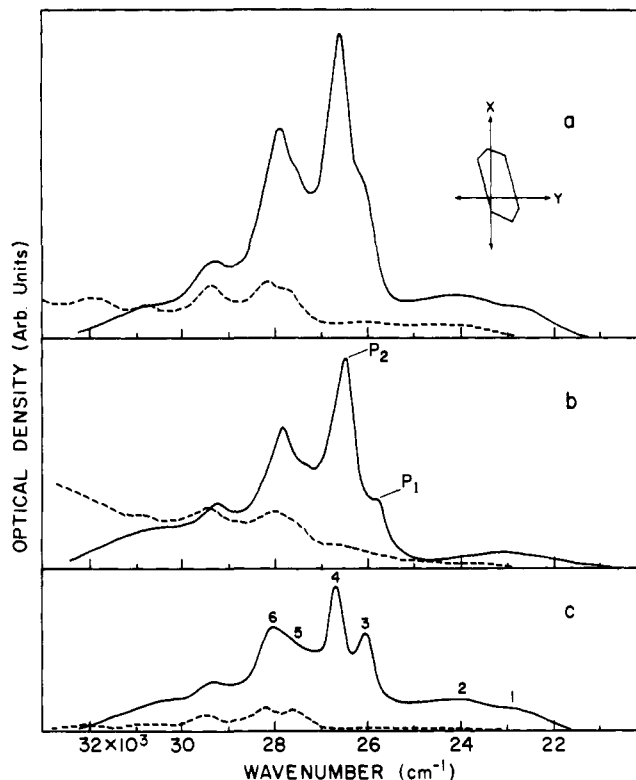


Figure 4. Absorption spectra (10K) of AEA in AEAPI for light incident normal to (010) face: (a) absorption after initial photodissociation; (b) absorption spectra of nonfluorescent AEA; (c) absorption spectra of fluorescent AEA. Full lines, polarization $\parallel X$; broken lines, polarization $\parallel Y$.

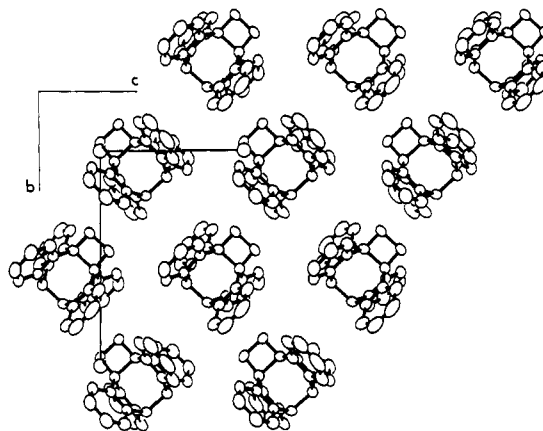


Figure 5. Projection of AEAPI molecules on (100) face.

which each of the two dissociated molecules in the unit cell would rotate to reduce the repulsion energy between it and its nearest neighbor ethane bridge, i.e., the molecule rotates into the "ethane hole" of its other neighboring molecule.

The orientations of the two nonfluorescent sets of molecules P_1 and P_2 in the lattice having been established, we consider their spectral features more closely. We note immediately that the spectra, for light incident normal to the (100) and (010) faces, enable a clear distinction to be made between long axis polarized transitions of the anthracene moieties on the one hand and short in-plane axis polarization and out-of-plane polarization on the other hand. We are unable to discriminate between the latter two directions.

It has already been established⁷ that the lattice constrained nonfluorescent conformations of photodissociated bridged anthracenes, very probably, have nonplanar anthracene chromophores with a geometry similar to that of [2.2]-(9,10)anthracenophane. Also, it is likely that the arrangement of the chromophores will not be symmetrical, so that the real symmetry of a conformation will be low, and states of different parentage might be mixed, particularly as a result of the enforced orbital overlap between the chromophores. It is therefore not at all surprising to find in the spectrum of the (001) face appreciable long-axis polarization. This absorption intensity extends to about 23 000 cm^{-1} on the low-energy side and it increases toward high energy, particularly above 30 000 cm^{-1} . Measurements with thin crystals established that this long absorption tail is associated with an absorption edge at about 35 000 cm^{-1} . This edge is removed by irradiation at 26 450 cm^{-1} and is therefore a property of the spectrum of the nonfluorescent molecules. We ascribe it to the nonplanar chromophore conformation.

Theories^{24,25} which describe the energy levels of two interacting anthracene molecules, in a sandwich arrangement, have assumed planarity of the molecules, so it is interesting to compare the true situation with the artificial one. These theories derived the energy levels from a consideration of the interaction between charge resonance (CR) and excitation resonance (ER) states of the dimer. With the assumption of D_{2h} symmetry for the dimer and, considering only the highest bonding MO and the lowest bonding MO of each molecule, there are four excited states of the dimer, belonging to the representations B_{3g}^- , B_{2u}^- , B_{2u}^+ , and B_{3g}^+ , in increasing order of energy (nomenclature of Azumi et al.²⁴).

Transitions from the ground state are allowed to B_{2u}^+ and B_{2u}^- for electric dipole absorption. The corresponding transition moments are given by the vector-sum (for B_{2u}^-) and vector difference (for B_{2u}^+) of the dimer ER moments and the CR moments. Transitions to the B_{3g}^- and B_{3g}^+ states are forbidden for the D_{2h} dimer. The splitting between B_{2u}^+ and B_{2u}^- states is expected to be small, while the splitting between B_{3g}^+ and B_{3g}^- states is much larger and very dependent on the intermolecular separation. The bandwidths of the transition to the latter states (in the absence of a center of symmetry) should therefore be much larger than the bandwidths of the transitions to the former states. The very weak and broad bandwidth maximum at about 23 000 cm^{-1} in Figures 3 and 4 is therefore assigned to the transition to B_{3g}^- . Its low intensity indicates the presence of a pseudocenter of symmetry between the two anthracene chromophores. The band is also probably associated with the rotated molecules P_2 .

The bands with origins P_1 and P_2 are then assigned either to B_{2u}^+ or B_{2u}^- and each has a 1400- cm^{-1} vibrational progression built on it. The difference between the energies of the two origins will involve differences in the destabilization of their ground states, as well as differences in their excited state interaction energies.

The remaining feature to consider is the long axis polarized intensity in the spectrum (Figure 4b). Apart from the structure between 27 500 and 32 000 cm^{-1} , there is an appreciable tail which extends to about 23 000 cm^{-1} . This long absorption tail, observed only for the nonfluorescent molecules, indicates that the electronic structure of the interacting nonplanar anthracene chromophores is not accurately described by the states of the planar molecules as might seem from the preceding analysis. There is no simple way in which intensity with this polarization can be derived from the interacting states of the planar anthracene molecule. It must be ascribed to the effect of a departure from planarity and requires a theoretical evaluation, outside the scope of the present work.

Apart from the extended absorption tail there is, superimposed on it, a structured absorption which, from its long-axis

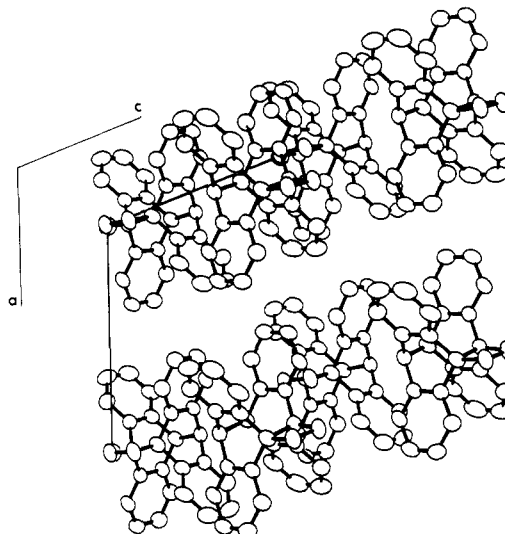


Figure 6. Projection of AEAP1 molecule on (010) face.

polarization, must be the otherwise hidden transition to the 1L_b (${}^1B_{3u}$) state of anthracene.

Turning now to the fluorescent molecules, we note (Figures 3c and 4c) that the essential difference between their spectra and those of the nonfluorescent molecules is the relatively large intensity of the bands below 25 000 cm^{-1} . As these bands can be assigned to the B_{3g}^- state of the dimer, it is clear that there is no longer a pseudocenter of symmetry. We take this as evidence that the planes of the anthracene moieties are no longer parallel. This corresponds to the second stage of relaxation mentioned above, i.e., an opening of the face to face contacts of the moieties about the ethane bridge.

The appearance of two bands in the low-energy region and two maxima at higher energy, near P_1 and P_2 , initially suggests that there are two types of molecules involved. However, there are three experimental observations which show that only one type of molecule is involved, but it has two conformational forms.

First, there is the effect of temperature on the absorption spectrum. An increase of temperature shifts bands 1, 3, and 5 to higher energy and they combine with bands 2, 4, and 6, respectively (see Figures 3 and 4 for numbering). At the same time bands 2, 4, and 6 show a small shift to lower energy. All of these shifts are reversible with temperature, so that on cooling the crystal the original spectrum is regained.

Second, excitation throughout the whole of the absorption spectrum, with narrow band excitation, gives rise to the same fluorescence spectrum. This indicates a common fluorescent state.

Third, attempts at selective photoisomerization using narrow band irradiation over the whole of the spectral range resulted in a uniform diminution of the overall spectral intensity. This result is, of course, consistent with the single fluorescence spectrum.

We have noted that these molecules undergo photoisomerization at about 10 K. An increase of temperature leads to an increase of the rate of photoisomerization, a decrease of the fluorescence intensity, and a decrease in the fluorescence decay rate. These observations indicate that there is a thermal barrier to photoisomerization and it is important to determine its value and whether it has an intramolecular origin.

In spite of repeated measurements of the temperature dependence of the various properties mentioned in the previous paragraph, we were unable to obtain a consistent measurement of the barrier. The values obtained varied from a few tens of cm^{-1} to a few hundreds of cm^{-1} . There appeared to be a gen-

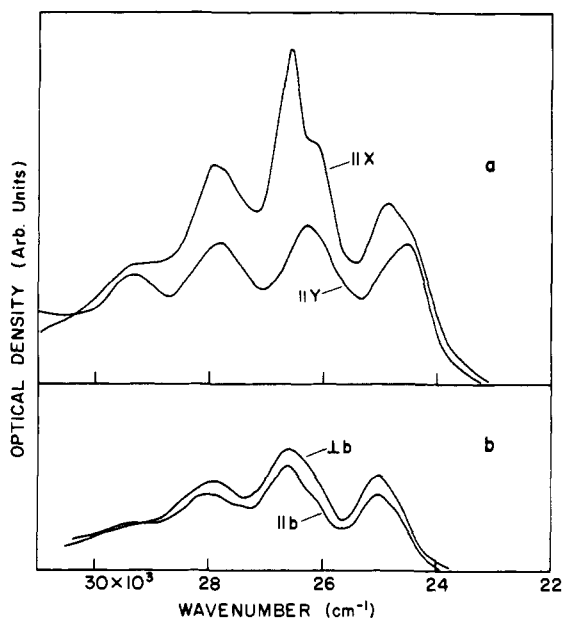


Figure 7. Absorption spectra of relaxed AEA in AEAPI single crystals: (a) absorption spectra for light incident normal to (010) face; (b) absorption spectra for light incident normal to (100) face.

eral correlation between low values and "aged" crystals and between high values and "fresh" crystals, which suggests that the barrier is related to the constraints imposed by the lattice.

It seems very probable that the relaxation involves a movement away from the nearly eclipsed conformation and that this involves the translation of one moiety along its long axis, so as to relieve the carbon-carbon repulsion forces between the faces. The difference between the two conformations could then involve a small secondary rotation about the intermoiety axis so that the long axes of the moieties are no longer parallel. This latter conformation would allow a dihedral angle close to zero while the other, because of larger π - π repulsion forces, might have a nonzero dihedral angle. We note, from the absorption spectra in Figures 3c and 4, that bands 2 and 4 are symmetrically placed with respect to the origin of the completely relaxed AEA molecule, while bands 1 and 3 are displaced to lower energy, perhaps indicating a destabilization of the ground state because of a nonzero dihedral angle.

Absorption of light by either conformation leads, by a process of radiationless decay, to the lowest excited state, corresponding to band 1. As the conformation is displaced from the eclipsed conformation necessary for photoisomerization to proceed, there is a small barrier to surmount. The height of this barrier appears to be determined by the repulsive interaction between the cleaved molecule and the surrounding host lattice molecules. Fluorescence and photoisomerization from the displaced conformation are then competitive processes.

Photocleavage of AEAPI by Strongly Absorbed Light

Irradiation of AEAPI at low temperatures by light which is not on the extreme long-wavelength edge of the absorption spectrum leads to absorption spectra which depend on the irradiation time. Initially, at low optical densities, the spectra are similar to those shown in Figures 3a and 4a. As the irradiation proceeds, another absorption transition, with a broad origin near 405 nm, develops and, after prolonged irradiation, it dominates the spectrum. This absorption corresponds to band C in Figure 1 of the earlier report.⁶

In order to investigate the conformations responsible for this absorption, we used 254-nm radiation from a low-pressure Hg

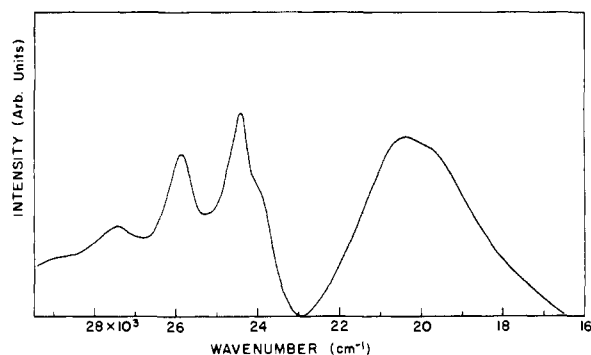


Figure 8. Excitation spectrum (left) and fluorescence spectrum (right) of AEA in "aged" AEAPI crystal.

lamp as a convenient source of strongly absorbed light. After a period of irradiation by 254-nm light, the crystals were then irradiated with various narrow bands of wavelengths from 380 to 440 nm to remove the fluorescent and nonfluorescent sites discussed in the previous section. The resultant spectra are shown in Figures 7a and 7b.

In order to understand these spectra, we made use of excitation spectra and fluorescence spectra excited by narrow band light from the double monochromator. These combined measurements reveal the presence of three different conformations of the relaxed molecule.

The first of these conformations has its origin at about $24\,500\text{ cm}^{-1}$, from the absorption spectra in Figure 7a. It is seen most clearly for light incident normal to the (010) face with intensity a little stronger in *Y* polarization. Irradiation with light in the region $24\,000$ – $24\,500\text{ cm}^{-1}$ produces fluorescence which has a broad spectrum with an intensity maximum at $20\,500\text{ cm}^{-1}$. The same fluorescence can be excited from aged AEAPI crystals so that these molecules are a product of thermal decomposition of the AEAPI. In some thick crystals their absorption can be detected directly, along with that of the completely relaxed molecules. We determined the absorption spectrum by measurement of the excitation spectrum of an aged AEAPI crystal. This is shown in Figure 8 along with the fluorescence spectrum. We note that as well as the maximum at $24\,500\text{ cm}^{-1}$ there is a shoulder near $24\,000\text{ cm}^{-1}$. We assign this shoulder to the out-of-phase dimer state and the $24\,500\text{-cm}^{-1}$ maximum to the in-phase dimer state and there must be a considerable angle between the (short axis) transition moments of the anthracene moieties. Although the fluorescence spectrum is broad and has "excimer" character, there is a very small gap between it and the absorption origin. In view of the presence of this molecule in aged AEAPI crystals, we assume that it has the most relaxed of the face-to-face conformations. If we consider a symmetrical rotation of the anthracene moieties about the ethane bridge in the relaxed cleaved molecule, then the polarization properties are consistent with the possible conformation for this site shown in Figure 9a.

The second relaxed conformation has an apparent origin at about $25\,000\text{ cm}^{-1}$ which is stronger in *Y* polarization of the (010) face. If this represents the in-phase dimer origin it is not possible to determine the lower energy out-of-phase dimer state because it is overlapped by the absorption due to the conformation just considered. Excitation near $24\,000\text{ cm}^{-1}$ gives a broad fluorescence band, shown in Figure 10. The polarization properties of the absorption bands are consistent with the conformation shown in Figure 9b.

The third relaxed conformation has a structured fluorescence spectrum, related to completely relaxed AEA present as an impurity in the crystals. However, whereas the latter has a relatively sharp origin at $25\,250\text{ cm}^{-1}$, this third relaxed set

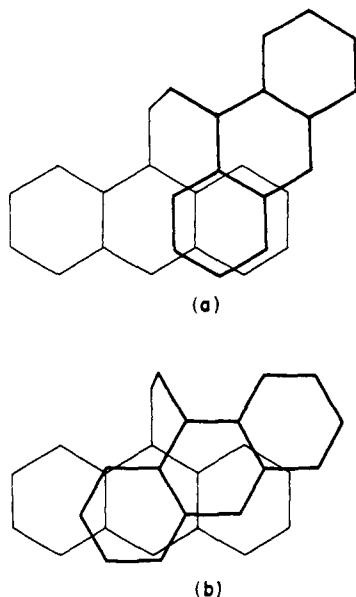


Figure 9. Possible conformations of relaxed AEA in AEAPI crystal (see text).

of molecules has a broader distribution of energies corresponding to a spread in its conformations. It is interesting to observe the variation in the fluorescence spectrum for narrow band excitation across the absorption band corresponding to these molecules. Figure 11 shows a series of such spectra.

The spectra in Figure 11 comprise overlapping contributions from broad and structured emissions, the latter due to the partially relaxed excimer considered previously. As the excitation wavelength is moved progressively to lower energy, we find that the structured component broadens and moves to lower energy.

The insert in Figure 11 shows the wavenumber gap between the excitation wavelength and the highest energy maximum observed in the structured emission (the first vibronic ground-state excitation of the 1400-cm^{-1} mode). As the excitation wavelength is increased, this wavenumber gap drops to a minimum and then rises again. The position of the minimum ($25\ 150\text{ cm}^{-1}$) must correspond to the pure electronic origin of the completely relaxed AEA. In this latter conformation the anthracene moieties are unable to return to a face-to-face or partial sandwich conformation (Figures 9a and b) during the lifetime of the excited state, because of lattice constraints. The fluorescence spectrum then has essentially no gap between its origin and the origin of the absorption spectrum.

It follows then that the important excited state relaxation which occurs after absorption of light is a decrease in the intramolecular separation between the planes of the anthracene moieties, which are already in a partial sandwich conformation in the ground state (Figure 9b through Figure 9a), toward a completely relaxed nonoverlapped conformation. The lowest excited state of each of these conformations can be lowered further through charge transfer between the two moieties because of the π - π overlap. The closer the conformation is to the sandwich conformation (Figures 9a to 9b), the more effective is the charge-transfer contribution to the energy level of the excited state, the greater is the energy gap between absorption and fluorescence, and the smaller becomes the interplanar separation. This is just the process of excited state relaxation which was proposed for the pyrene excimer,²⁶ the essential difference between the present case and pyrene being that the lattice constraints provide a range of conformations for the former, while there is only one for the latter. The pyrene dimer

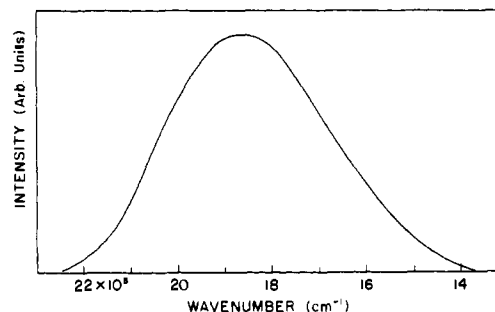


Figure 10. Fluorescence spectrum of relaxed AEA in AEAPI crystal, excited by $24\ 000\text{-cm}^{-1}$ light, probably with conformation of Figure 9b.

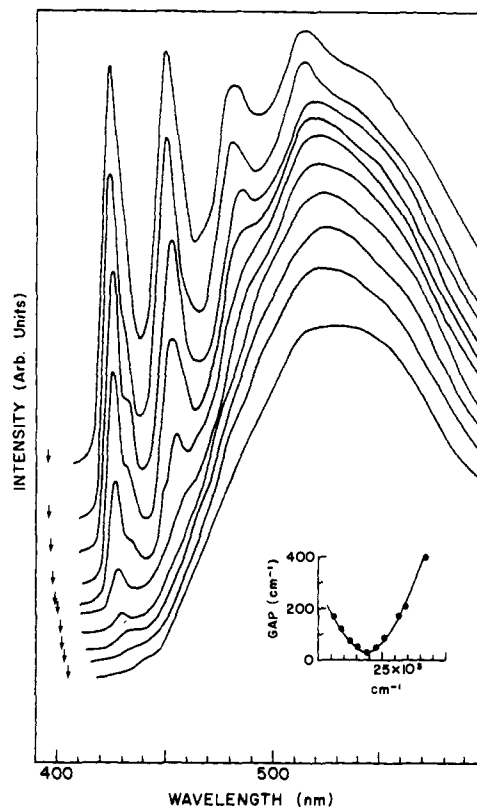


Figure 11. Series of fluorescence spectra showing transition from structured to nonstructured spectrum as the excitation wavelength is moved to larger wavelength (arrows denote excitation wavelength). Insert shows wavenumber gap between excitation wavelength and highest energy maximum of the structural emission (see text).

can reach its lowest possible minimum excited state level simply by a reduction of the interplanar spacing because the ground-state geometry is close to a completely eclipsed one.

The spectra in Figure 11 then provide evidence for the process of excited state relaxation which leads to excimer characteristics in the fluorescence of the excited dimer. There is essentially a continuous range of energy levels corresponding to a continuous range of conformations involving the face-to-face geometry of the anthracene moieties. These solid-state results confirm the similar conclusions reached earlier from studies²⁷ of the fluorescence from sandwich dimers in rigid glasses as the glasses were allowed to soften. Entirely analogous results have also been obtained for the partially relaxed sites in the cleaved, 1,3-di(9-anthryl)-(1-naphthyl)propane.²⁸

Thermal Dissociation of AEAPI

AEAPI is thermally unstable and the crystals develop, even when placed in a refrigerator, a blue-green fluorescence a few

days after preparation. The absorption and emission spectra of the products are the same as those which can be obtained by photodissociation with strongly absorbed light, as discussed above.

Presumably the sites at which thermal cleavage occur are in the neighborhood of inhomogeneities in the crystal lattice, such as dislocations, impurities, and included solvent molecules. There are two observations to support this hypothesis. First, we noted that the crystals obtained for benzene-methylcyclohexane are more unstable than are the crystals obtained from dichloromethane, perhaps as a result of the inclusion of small amounts of benzene in the former solvent. Certainly the role of the solvent in determining the crystal habit could support the possibility of solvent inclusion. Second, we tried unsuccessfully to use AEAPI as a host crystal for the inclusion of [2.2](1,4)(9,10)anthracenophane for a spectral study of the latter. However, these crystals always had a large amount of relaxed AEA in them, as much as two orders of magnitude more than the crystals usually obtained. We concluded that the presence of the impurity in the lattice catalyzes the thermal cleavage of AEAPI.

These observations suggest that thermal studies of the cleavage of AEAPI in its crystalline form will be sample dependent, so that a more simple, but tedious technique, was used to determine the activation barrier to thermal cleavage. In this method the rate of formation of AEA, at a fixed temperature, was determined by measuring its absorption spectrum as a function of time. The solvent used was *n*-hexane. The analysis of these results, in the form of an Arrhenius plot, provides a barrier of 25.85 kcal/mol and a frequency factor of 2.1×10^{10} . The larger value obtained by Bergmark and Jones⁸ for the barrier indicates the need to exercise care in obtaining these parameters from measurements in the solid state (see also Mau²⁹).

Supplementary Material Available: A listing of structure factor amplitudes and of atomic thermal parameters (6 pages). Ordering information is given on any current masthead page.

References and Notes

- (1) (a) Department of Chemistry, Biochemistry and Biophysics, Massey University, Palmerston North, New Zealand; (b) Research School of Chemistry, Australian National University, Canberra, A.C.T., Australia; (c) Department of Chemistry, Faculty of Science, Nagoya University, Chikusa, Nagoya, Japan.
- (2) R. Livingston and K. S. Wei, *J. Am. Chem. Soc.*, **89**, 3098-3100 (1967).
- (3) I. Roitt and W. Waters, *J. Chem. Soc.*, 2695-2705 (1952).
- (4) T. Hayashi, T. Suzuki, N. Mataga, Y. Sakata, and S. Misumi, *Chem. Phys. Lett.*, **38**, 599-601 (1976).
- (5) T. Hayashi, N. Mataga, Y. Sakata, S. Misumi, M. Morita, and J. Tanaka, *J. Am. Chem. Soc.*, **98**, 5910-5913 (1976).
- (6) J. Ferguson, M. Morita, and M. Puza, *Chem. Phys. Lett.*, **42**, 288-292 (1976).
- (7) J. Ferguson, M. Morita, and M. Puza, *Chem. Phys. Lett.*, **49**, 265-268 (1977).
- (8) W. R. Bergmark and G. Jones, II, *Nouv. J. Chim.*, **1**, 271-275 (1977).
- (9) J. Ferguson and M. Puza, *Chem. Phys. Lett.*, **53**, 215-218 (1978).
- (10) J. Ferguson, *The Spex Speaker*, **21** (No. 1) (1976).
- (11) J. Ferguson and S. E. H. Miller, *Chem. Phys. Lett.*, **36**, 635-638 (1975).
- (12) The programs contained in the Picker Corp. FACS-1 disk operating system (1972) were used for all phases of diffractometer control and data collection.
- (13) The structure amplitude ($|F_o|$) is calculated from $|F_o| = \{(\lambda Lp)^{-1}\}^{1/2}$, where I (the net peak count) = $(CT - (t_p/t_b)(B_1 + B_2))$, Lp (the Lorentz-polarization correction) = $(\cos^2 2\theta + \cos^2 2\theta_m) / \sin 2\theta(1 + \cos^2 2\theta_m)$, and the remaining symbols have the following significance: CT is the total reflection count uncorrected for background, t_p and t_b are reflection and total background counting times, B_1 and B_2 are individual background counts (each in time $t_b/2$), and θ and θ_m are specimen and monochromator Bragg angles, respectively.
- (14) $\sigma(F_o) = \{[\sigma(I)/(Lp)]^2 + \rho^2 |F_o|^4\}^{1/2} / 2 |F_o|$, where $\sigma(I) = [CT + (t_p/t_b)^2(B_1 + B_2)]^{1/2}$ and ρ^2 is the instrumental uncertainty constant.¹⁵
- (15) W. R. Busing and H. A. Levy, *J. Chem. Phys.*, **26**, 563-568 (1957); P. W. R. Corfield, R. J. Doedens, and J. A. Ibers, *Inorg. Chem.*, **6**, 197-204 (1967).
- (16) G. Germain, P. Main, and M. M. Woolfson, *Acta Crystallogr., Sect. A*, **27**, 368-376 (1971).
- (17) M. Ehrenberg, *Acta Crystallogr.*, **20**, 183-186 (1966).
- (18) "International Tables for X-ray Crystallography", Vol. IV, Kynoch Press, Birmingham, England, 1974, pp 72-73.
- (19) J. Ferguson, A. W-H. Mau, and P. O. Whimp, *J. Am. Chem. Soc.*, in press.
- (20) J. Gaultier, C. Hauw, J. P. Desvergene, and R. Lapouyard, *Cryst. Struct. Commun.*, **4**, 497-500 (1975).
- (21) A. Dunand, J. Ferguson, and G. B. Robertson, unpublished observations.
- (22) (a) *Chem. Soc. Spec. Publ.*, No. 18, S14s (1965); (b) *ibid.*, No. 18, S15s (1965).
- (23) X, Y, and Z are orthonormal coordinates: $X = 10.095(x/a) - 3.017(z/c)$, $Y = 12.471(y/b)$, $Z = 7.775(z/c)$.
- (24) T. Azumi, A. T. Armstrong, and S. P. McGlynn, *J. Chem. Phys.*, **41**, 3839-3852 (1964).
- (25) J. N. Murrell and J. Tanaka, *Mol. Phys.*, **7**, 363-380 (1964).
- (26) J. Ferguson, *J. Chem. Phys.*, **28**, 765-768 (1958).
- (27) J. Ferguson, A. W-H. Mau, and J. M. Morris, *Aust. J. Chem.*, **26**, 91-102 (1973).
- (28) J. Ferguson, A. W-H. Mau, and P. O. Whimp, *J. Am. Chem. Soc.*, in press.
- (29) A. W-H. Mau, *J. Chem. Soc., Faraday Trans. 1*, 603 (1978).